COMPUTER MODELING OF ANTENNAS NEAR THE GROUND

G. J. Burke, E. K. Miller, J. N. Brittingham, D. L. Lager, R. J. Lytle, and J. T. Okada, *Lawrence Livermore National Laboratory, University of California Livermore, CA 94550*

ABSTRACT

An accurate and efficient numerical method based on the rigorous Sommerfeld theory is described for modeling antennas near an interface such as the ground. The Sommerfeld integrals are evaluated by numerical integration along contours in the complex plane and two-dimensional interpolation is used subsequently to obtain the many Sommerfeld integral values needed for the moment-method solution of an integral equation. These methods permit modeling an antenna within 10^{-6} wavelengths of the ground for about two to four times the computation time for the same antenna in free space. Results showing currents and radiation patterns are included.

1. INTRODUCTION

A problem that has traditionally resisted a genuinely practical solution despite considerable longevity and study is that of modeling conducting structures (antennas or scatterers) located near a planar interface such as the earth's surface. More than 70 years ago, Sommerfeld (1909) worked out the basis for the rigorous solution of this problem in terms of Fourier integrals of cylindrical wave expansions. These Sommerfeld integrals have been studied extensively and numerous approximations have been developed for them involving various combinations of the problem's parameters [see Banos (1966) for example]. However, the evaluation of the Sommerfeld integrals for the ranges of source and observation-point locations that typically must be covered for any self-consistent description of the structure's current - an integral equation for example - almost inevitably involves some parameter combinations to which such approximations do not apply. Consequently, the only feasible approach for obtaining a reliable, straightforward solution has been to integrate the Sommerfeld integrals numerically, which can be a computationally inefficient process.

Work performed under the auspices of the U.S. Department of Energy by the Lawrence Livermore National Laboratory under contract number W-7405-ENG-48.

Electromagnetics 1:29-49, 1981
0272-6343/81/010029-21$2.25

In this paper we present a recently developed procedure for Sommerfeld--integral evaluation which preserves the rigor and generality of numerical integration, while achieving the efficiency and simplicity of asymptotic techniques. Its successful implementation depends primarily on two factors. First, it is necessary to have a valid numerical algorithm for evaluating Sommerfeld integrals, a topic to which a separate Section (3) is devoted. Second, the number of Sommerfeld-integral values subsequently required is reduced to a minimum, as is the computation time consequently, by employing an interpolation procedure, [Brittingham, Miller and Okada (1977)] which is outlined in Section 4. These two factors together, when combined with an integral equation treatment (outlined in Section II), provide an accurate technique for modeling antennas near the ground (within 10^{-6} wavelength) which is little more costly in computer time (2 to 4 times) than the free-space problem. Capabilities, limitations and representative results of this technique are given in Section 5.

2. MODELING ANTENNAS NEAR GROUND

The use of integral-equation techniques for treatment of radiation and scattering problems is well known. These techniques involve the formulation of an integral expression for the fields of volume, surface or line distributions of sources. The expression becomes an integral equation upon imposition of appropriate boundary conditions which include the exciting field or source. The integral equation is subsequently reduced to an Nth order linear system via the moment method, whereby the current is expanded in a sum of N basis functions and the boundary condition is enforced on N (or more) weighted integrals of the field. The solution can then be obtained numerically by standard matrix methods.

The computational effort required to apply the moment-method procedure is intimately related to the kernel of the integral operator and the dimensionality of the associated integration. Wire integral equations are most commonly used since, among other factors, they involve a one-dimensional integration and lead to a matrix whose order is linearly proportional to the total length of wire measured in wavelengths. They have, in particular, been used extensively for free-space application.

A typical wire integral equation [Miller and Deadrick (1975)] can be written

$$-\hat{s}\cdot\vec{E}^{I}(\vec{r}) = \int_{C} I(s')\,\hat{s}'\cdot\bar{\bar{G}}_{D}(\vec{r},\vec{r}')\cdot\hat{s}\,ds',\quad \vec{r}\in\vec{C}(s) \tag{1}$$

where I is the induced current, $\vec{E}^{I}$ is the exciting field, $\hat{s}$ and $\hat{s}'$ are unit vectors tangent to the wire at s and s', and r and r' are vectors to the points $\vec{s}$ and $\vec{s}'$ on the wire contour $\vec{C}$. $\bar{\bar{G}}_{D}$ is the dyadic Green's function for the electric field at $\vec{r}$ due to a current element at $\vec{r}'$. The thin wire approximation is used so that the minimum separation between $\vec{r}$ and $\vec{r}'$ is the wire radius.

The numerical solution of Eq. (1) is relatively straightforward using available numerical methods and computers. Its reduction to matrix form involves several common steps whatever the specific approach (e.g., introduction of basis and weight functions, matrix manipulation, etc.). The approach we have used includes the following: (1) approximating the wire contour $\vec{C}(s)$ as a piecewise linear sequence of N segments of length Δ_i i=1, ..., N. (2)

using a subsectional basis over segment i of the form $I_i(s') = A_i + B_i \sin[k(s'-s_i)] + C_i \cos[k(s'-s_i)]$ where k is the free-space wave number, while imposing current and charge continuity at junctions; (3) evaluating the field at the center of each segment using delta-function weights $\sigma(s-s_j)$, j=1, ...N; (4) specifying the exciting field tangent to each segment; (5) inverting or factoring the matrix; (6) solving for the basis function amplitudes and total current to compute the fields.

The total computer solution time is well approximated by $AN^2 + BN^3$, where A corresponds to step (3) and B to step (5). For the code under consideration here and for a CDC 7600 computer, $A \approx 4 \times 10^{-4}$s and $B \approx 2 \times 10^{-6}$s for free space, so that a 10-wavelength dipole antenna, for example, requires $\lesssim$ 2s of computer time, for 6 segments per wavelength.

Extension of Eq. (1) to the case of a perfect ground plane by including the image in the Green's function results in no appreciable complication in the formulation, and calculation time for step 3 is increased by a factor of about two.

Analysis of the imperfect or lossy ground plane is another matter. If an image-theory approach is employed, the ground-reflected fields are approximated by their perfect-ground image fields decomposed into transverse electric and magnetic components and multiplied by their respective Fresnel plane-wave reflection coefficients evaluated at the specular reflection point [Miller, Poggio, Burke and Selden (1972)]. This procedure is only slightly more involved than that used for the perfect ground, but can lead to invalid results for antennas that are closely coupled to the ground. Rigorous treatment of the lossy ground plane requires instead that we employ the Sommerfeld integrals or their equivalent in the integral-equation kernel.

Eq. (1) can then take the form

$$-\hat{s} \cdot \vec{E}^I_G(\vec{r}) = \int_C I(s')\, \hat{s}' \cdot \left[\bar{\bar{G}}_D(\vec{r}, \vec{r}') + \bar{\bar{S}}(\vec{r}, \vec{r}')\right] \cdot \hat{s}\, ds' \qquad (2)$$

where $\bar{\bar{G}}_D$ is the free space field and $\bar{\bar{S}}$ combines components of the image field for a perfect ground with Sommerfeld integrals which account for ground loss. $\vec{E}^I_G$ is the incident or applied field in the presence of ground. Since the Sommerfeld integrals generally require numerical integration, we must contend with a two-dimensional integral in order to solve Eq. (2). This accounts for the great increase in computer time (a factor of $\gtrsim 10^2$) required for its solution compared to the free-space problem if the Sommerfeld integral values in $\bar{\bar{S}}$ come from direct numerical integration. It is for this reason that the interpolation procedure we developed to provide indirectly the many values of $\bar{\bar{S}}$ needed in Eq. (2) is so necessary if practical application of the Sommerfeld formulation is to be realized. But the interpolation procedure could not itself be implemented without a dependable way of obtaining directly the small number of $\bar{\bar{S}}$ values it requires. Our approach to compute these $\bar{\bar{S}}$ values is described in the next section.

3. COMPUTING SOMMERFELD INTEGRALS

3.1. Analytical Background

In the integral Eq. (2) above, we have indicated in only a symbolic fashion the Sommerfeld-integral contribution which arises because of finite ground conductivity and which includes a correction to the image field of a perfect ground plane. Our concern in this section is to discuss the specific form of the Sommerfeld integrals, their analytic properties and our approach to their numerical computation. Because the image and Sommerfeld terms in $\bar{S}$ can be combined in various ways, the Sommerfeld integrals have no unique form. It is important therefore, for understanding our approach, to show explicitly the field expressions we have employed.

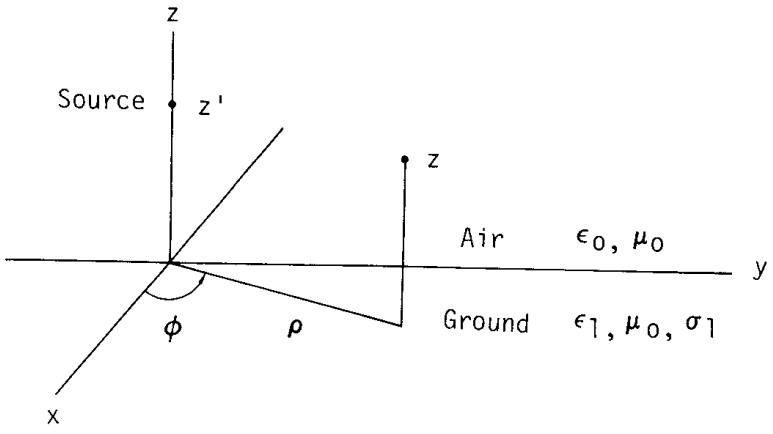

Fig. 1. Coordinates for Evaluating the Field of a Current Element Over Ground.

We begin using Banos (1966) notation for the fields above an air-ground interface of an infinitesimal current element of strength $I\ell$ also above the interface, with parameters shown in Fig. 1. The field is given by the following expressions:

$$E_\rho^V = C_1 \frac{\partial^2}{\partial\rho\partial z}\left[G_{22} - G_{21} + k_1^2 V_{22}\right], \tag{3a}$$

$$E_z^V = C_1\left(\frac{\partial^2}{\partial z^2} + k_2^2\right)\left(G_{22} - G_{21} + k_1^2 V_{22}\right), \tag{3b}$$

$$E_\rho^H = C_1 \cos\phi\left[\frac{\partial^2}{\partial\rho^2}\left(G_{22} - G_{21} + k_2^2 V_{22}\right) + k_2^2\left(G_{22} - G_{21} + U_{22}\right)\right], \tag{3c}$$

$$E_\phi^H = -C_1 \sin\phi\left[\frac{1}{\rho}\frac{\partial}{\partial\rho}\left(G_{22} - G_{21} + k_2^2 V_{22}\right) + k_2^2\left(G_{22} - G_{21} + U_{22}\right)\right], \tag{3d}$$

$$E_z^H = C_1 \cos\phi \frac{\partial^2}{\partial z \partial \rho}\left(G_{22} + G_{21} - k_1^2 V_{22}\right), \tag{3e}$$

$$C_1 = \frac{-j\omega I \ell \mu_0}{4\pi k_2^2},$$

$$k_1^2 = \omega^2 \mu_0 \varepsilon_0 \left(\frac{\varepsilon_1}{\varepsilon_0} - \frac{j\sigma_1}{\omega\varepsilon_0}\right),$$

$$k_2^2 = \omega^2 \mu_0 \varepsilon_0 ,$$

where the superscript indicates a vertical (V) or horizontal (H) current element and the subscript indicates the cylindrical component of the field vector. The horizontal current element is along the x axis.

G_{22} and G_{21} are the free space and image Green's functions

$$G_{22} = \exp(-jk_2R_2)/R_2,$$

$$G_{21} = \exp(-jk_2R_1)/R_1,$$

where

$$R_1 = \left[\rho^2 + (z+z')^2\right]^{1/2},$$

$$R_2 = \left[\rho^2 + (z-z')^2\right]^{1/2},$$

and U_{22} and V_{22} are Sommerfeld integrals involving the zeroth order Bessel function, J_0

$$U_{22} = 2\int_0^\infty \frac{\exp[-\gamma_2(z + z')]\, J_0(\lambda\rho)\lambda d\lambda}{\gamma_1 + \gamma_2}, \tag{4a}$$

$$V_{22} = 2\int_0^\infty \frac{\exp[-\gamma_2(z + z')]\, J_0(\lambda\rho)\lambda d\lambda}{k_1^2\gamma_2 + k_2^2\gamma_1}, \tag{4b}$$

where

$$\gamma_1 = \left(\lambda^2 - k_1^2\right)^{1/2},$$

$$\gamma_2 = \left(\lambda^2 - k_2^2\right)^{1/2}.$$

The field components of Eq. (3) can be used to construct $\bar{\bar{G}}_D$ and $\bar{\bar{S}}$ of Eq. (2) by decomposing the fields of $\hat{x}$, $\hat{y}$, and $\hat{z}$ directed current elements at r' into their cartesian components. Numerical integration over the product of the current and Green's function in Eq. (2) could, however, encounter computational difficulty due to the singularities in the various field components. For example, G_{22} of Eq. (3) has a $1/R_2$ singularity while G_{21}, U_{22} and V_{22} each

have $1/R_1$ singularities. Furthermore, the derivatives in the field expressions result in higher order $1/R^3$ singularities which produce a triplet-like behavior in the field components parallel to the current element. Thus, for a horizontal wire at height h above the ground, the peak of the kernel is proportional to h^{-3} (i.e., to $1/R^3$). Due to cancellation, the contribution of the singular region to the integral for the tangential field increases as log (h). Similarly, the effect of errors in numerical integration of Eq. (2) and in the values obtained for the Sommerfeld integrals increases as h^{-2} since integrating a $1/R^3$ function without cancellation gives a $1/R^2$ result. As h is reduced this leads to a critical accuracy requirement that may limit the minimum height for which a wire can be modeled.

3.2 Reducing the Order of the Singularities

The problem of numerically integrating such high-order singularities can be alleviated significantly if, by analytic means, the order of the singularity can be reduced. One way to accomplish this is to subtract an analytically integrable singular function from the integral. A convenient analytically integrable function is provided by the free-space Green's dyad $\bar{\bar{G}}_D$ which when multiplied in Eq. (2) by a sinusoidal current yields a closed form result for the field [Miller and Deadrick (1975)]. For a constant current the field in free space involves numerical integration of only the $1/R_2$ function G_{22} for which the integral and the effect of errors are on the order of the logarithm of the minimum value of R_2.

The $1/R_1^3$ singularity in the Sommerfeld integral terms in $\bar{\bar{S}}$ results from the second derivatives of V_{22} which, itself, has a $1/R_1$ singularity. This high-order singularity can be isolated in a term proportional to the free-space field of the image by introducing the modified Sommerfeld integrals

$$U'_{22} = \int_0^\infty D_1 \exp\left[-\gamma_2 (z+z')\right] J_0(\lambda\rho)\, \lambda\, d\lambda = U_{22} - \frac{2k_2^2}{k_1^2 + k_2^2} G_{21} \tag{5a}$$

$$V'_{22} = \int_0^\infty D_2 \exp\left[-\gamma_2 (z+z')\right] J_0(\lambda\rho)\, \lambda\, d\lambda = V_{22} - \frac{2}{k_1^2 + k_2^2} G_{21} \tag{5b}$$

where

$$D_1 = \frac{2}{\gamma_1 + \gamma_2} - \frac{2k_2^2}{\gamma_2 (k_1^2 + k_2^2)}, \tag{6a}$$

$$D_2 = \frac{2}{k_1^2 \gamma_2 + k_2^2 \gamma_1} - \frac{2}{\gamma_2 (k_1^2 + k_2^2)}. \tag{6b}$$

and the relation

$$\int_0^\infty \gamma_2^{-1} \exp\left[-\gamma_2 (z+z')\right] J_0(\lambda\rho)\, \lambda\, d\lambda = G_{21}$$

has been used.

When Eqs. (5) are substituted into Eqs. (3), the terms involving G_{21} in each field component are the field of the image multiplied by $(k_1^2 - k_2^2)/(k_1^2 + k_2^2)$. Thus the dyadic Green's function constructed from these components can be written as

$$\bar{\bar{G}}_D(\vec{r}, \vec{r}') + \bar{\bar{S}}(\vec{r}, \vec{r}') =$$

$$\bar{\bar{G}}_D(\vec{r}, \vec{r}') + \frac{k_1^2 - k_2^2}{k_1^2 + k_2^2}\, \bar{\bar{G}}_I(\vec{r}, \vec{r}') + \bar{\bar{S}}'(\vec{r}, \vec{r}') \tag{7}$$

where $\bar{\bar{G}}_I$ is the free space Greens dyad for the image of the source. Eq. 3, by contrast, has the form of a direct field plus image plus Sommerfeld in Eqs. c and d and a direct field minus image plus Sommerfeld in Eqs. a, b, and e.

The advantage of Eq. 7 is that the Sommerfeld integral terms in $\bar{\bar{S}}'$ have only $1/R_1$ singularities. The integral for V'_{22} converges as ρ and $z+z'$go to zero, while second derivatives of V_{22} in the field expressions have $1/R_1$ singularities. The term subtracted from U_{22} does not alter its $1/R_1$ singularity but completes the second term on tne right hand side of Eq. 7 in the form of the free-space field of the image. Thus, 1/R3 singularities occur only in $\bar{\bar{G}}_D$ and $\bar{\bar{G}}_I$ which, since they are free-space fields, can be easily integrated for sinusoidal or constant currents. The $1/R_1$ functions in $\bar{\bar{S}}'$ can be integrated numerically for a wire very close to the interface since the integral and the effect of errors both go as log(h). (The $1/R_1$ singularity could also be integrated analytically by subtracting Eq. 11 from Eq. 9, [see Section IV], but this was not found to be necessary.)

The field components for $\bar{\bar{S}}'$ corresponding to Eq. 3 are

$$E_\rho^{'V} = C_1 \frac{\partial^2}{\partial\rho\partial z} k_1^2 V'_{22}\,, \tag{8a}$$

$$E_z^{'V} = C_1\left(\frac{\partial^2}{\partial z^2} + k_2^2\ \ k_1^2 V'_{22}\right), \tag{8b}$$

$$E_\rho^{'H} = C_1 \cos\phi \left(\frac{\partial^2}{\partial\rho^2} k_2^2 V'_{22} + k_2^2 U'_{22}\right), \tag{8c}$$

$$E_\phi^{'H} = -C_1 \sin\phi \left(\frac{1}{\rho}\frac{\partial}{\partial\rho} k_2^2 V'_{22} + k_2^2 U'_{22}\right), \tag{8d}$$

$$E_z^{'H} = -\cos\phi\, E_\rho^{'V}. \tag{8e}$$

To evaluate these fields the derivatives are taken inside the U'_{22} and V'_{22} integrals leading to the following six integrals that require numerical evaluation.

$$\frac{\partial^2 V'_{22}}{\partial \rho^2} = \int_0^\infty D_2 \exp\left[-\gamma_2(z + z')\right] J_0''(\lambda\rho)\lambda^3 d\lambda\,, \tag{9a}$$

$$\frac{\partial^2 V'_{22}}{\partial z^2} = \int_0^\infty D_2\, \gamma_2^2 \exp\left[-\gamma_2(z + z')\right] J_0(\lambda\rho)\lambda d\lambda\,, \tag{9b}$$

$$\frac{\partial^2 V'_{22}}{\partial \rho \partial z} = -\int_0^\infty D_2\gamma_2 \exp\left[-\gamma_2(z + z')\right] J_0'(\lambda\rho)\lambda^2 d\lambda\,, \tag{9c}$$

$$\frac{1}{\rho}\frac{\partial V'_{22}}{\partial \rho} = \frac{1}{\rho}\int_0^\infty D_2 \exp\left[-\gamma_2(z + z')\right] J_0'(\lambda\rho)\lambda^2 d\lambda\,, \tag{9d}$$

$$V'_{22} = \int_0^\infty D_2 \exp\left[-\gamma_2(z + z')\right] J_0(\lambda\rho)\lambda d\lambda\,, \tag{9e}$$

$$U'_{22} = \int_0^\infty D_1 \exp\left[-\gamma_2(z + z')\right] J_0(\lambda\rho)\lambda d\lambda\,, \tag{9f}$$

The integrals in Eqs. (9a) through (9f) are evaluated by numerical integration along contours in the complex λ plane. Although these integrals differ from the usual Sommerfeld integrals in the D_1 and D_2 terms, they are the same in the properties important to numerical integration - the locations of poles and branch cuts and the behavior of the Bessel and exponential functions. The behavior of the integrands and numerical methods for evaluating the integrals are discussed in detail by Lytle and Lager (1974), and are described briefly here.

An alternate approach for computing Sommerfeld integrals, also based on manipulation of the integrand and integration contour, is reported elsewhere in this issue [Rahmat-Samii, Mittra and Parhami (1980)].

3.3. Numerical Treatment

Since the integrands of the six integrals are similar, V'_{22} will be considered as typical. The integrands have branch cuts from $\pm k_1$ to infinity and $\pm k_2$ to infinity due to the square roots in γ_1 and γ_2 respectively. The branch cuts are chosen to be vertical, as shown in Fig. 2.

The key to rapid convergence in the numerical integration is to exploit the exponential behavior of both the exponential and Bessel functions for large λ. The integration contour is deformed from the real axis into the complex plane, avoiding branch cuts and taking account of poles, to optimize convergence. With the vertical branch cuts chosen, there are no real poles on the primary Reimann sheet although virtual poles from D_1 or D_2 result in a near singularity in the region of $\pm k_2$ when k_1 approaches k_2 (free-space limit). Hence the integration contour should avoid the real axis in this region.

The contour used with the form of the integrals in Eqs. (9a) through (9f) is shown in Fig 2. The dominant factor for convergence in this case is the exponential function as λ_R increases. The Bessel function oscillates with slow convergence for increasing λ_R and grows exponentially as $|\lambda_I|$ increases. Hence it is of little help in convergence but restricts the contour to small $\rho|\lambda_I|$. The break in the contour is at $\lambda = p + jp$ where p is the minimum of $1/\rho$ and $1/(z+z')$.

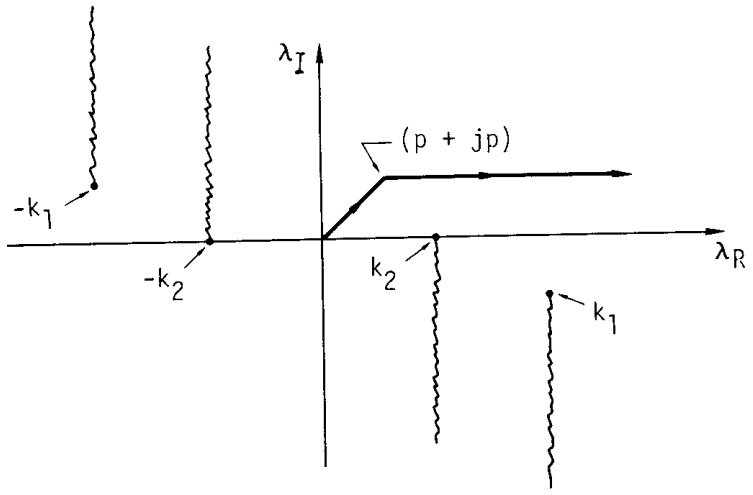

Fig. 2. Contour for Evaluation of Bessel Function Form of Sommerfeld Integrals.

Integration along this contour becomes difficult when $(z+z')/\rho$ is small since there may be many oscillations of the Bessel function before convergence. In this case an alternate form of the integrals is used, which for V'_{22} is

$$V'_{22} = \frac{1}{2} \int_{-\infty}^{\infty} D_2 \exp\left[-\gamma_2(z + z')\right] H_0^{(2)}(\lambda\rho)\lambda d\lambda \ . \qquad (9g)$$

Since the Hankel function of type 2 decays exponentially as λ_I becomes negative, it provides rapid convergence without the $\exp\left[-\gamma_2(z+z')\right]$ factor. The behavior of the integrand can be seen from the large argument approximation

$$\exp\left[-\gamma_2 (z + z')\right] H_0^{(2)}(\lambda\rho) \approx \sqrt{\frac{2j}{\pi\lambda\rho}} \{\exp -\lambda [\pm (z + z') + j\rho] \},$$

where, for the vertical branch cuts, the $\pm$ sign is

+ for $\lambda_R > -k_2$ and $\lambda_I > 0$,
+ for $\lambda_R > k_2$ and $\lambda_I < 0$,
- otherwise.

Thus, an integration path having

$$\lambda_I < 0$$

and

$$\lambda_I/\lambda_R \approx -\rho/(z + z') \text{ for } \lambda_R > k_2$$

or

$$\lambda_I/\lambda_R \approx \rho/(z + z') \text{ for } \lambda_R < k_2$$

results in exponential convergence with little oscillation. The basic contour used with the Hankel function form is shown in Fig. 3 where

$$a = -j\ 0.4\ k_2,$$
$$b = (0.6 + j\ 0.2)k_2,$$
$$c = (1.02 + j\ 0.2)k_2,$$
$$d = 1.01\ k_{1R} + j\ 0.99\ k_{1I},$$
$$\theta = \tan^{-1}\left(\frac{\rho}{z+z'}\right)$$

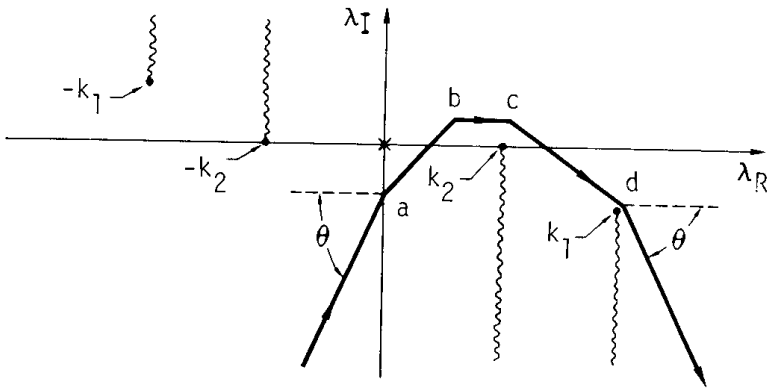

Fig. 3. Contour for Evaluation of Hankel Function Form of Sommerfeld Integrals.

To avoid the near singularity as k_1 approaches k_2, the real part of d is not allowed to be less than $1.1\ k_2$. This contour provides rapid convergence except when z+z' is small, $|k_1\rho|$ is large, and k_{1I}/k_{1R} is small. There may then be many oscillations between c and d with little convergence. In such a case the contour in Fig. 4 is used where

$$e = k_1 + (-0.1 + j\ 0.2),$$
$$f = k_1 + (0.1 + j\ 0.2).$$

The Hankel function form of the integrals provides rapid convergence for small z+z' including the case of $z=z' = 0$. For small ρ, however, the pole at $\lambda\rho = 0$ requires special treatment. Hence, the Hankel function form with the contour of Figs. 3 or 4 is used when ρ is greater than $(z+z')/2$ and the Bessel function form is used otherwise.

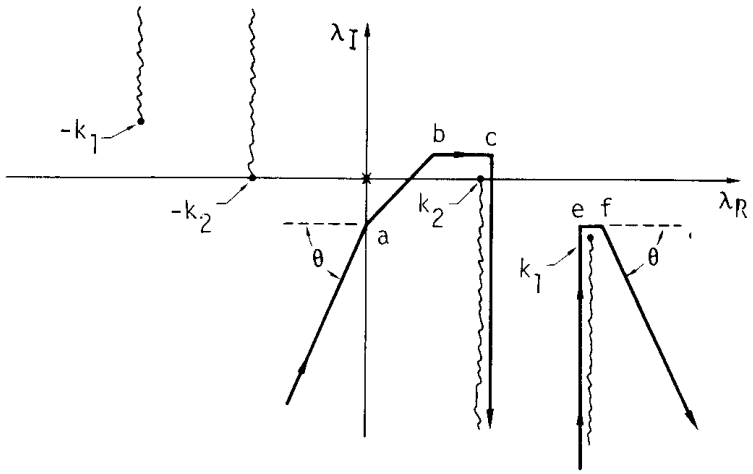

Fig. 4. Contour of Hankel Function Form when Real Part of k_1 is Large and Imaginary Part of k_1 is Small.

Integration along the contours is accomplished by adaptive interval-width Romberg integration [Miller (1970)]. On the sections going to infinity, adaptive Romberg integration is applied to successive subsections of length p, where p is the minimum of $0.2\pi/\rho$ or $0.2\pi/(z+z')$, and Shanks' (1955) nonlinear transformation is applied to the sequence of partial sums to accelerate convergence. When ρ and $z+z'$ are both small, the integration interval, p, may be large since the exponential and Bessel functions change slowly and the remaining factors are easily integrated once λ becomes large. For the Bessel function form of the integrals, the minimum value which can be used for $R_1 = [\rho^2 + (z+z')^2]^{1/2}$ is limited by computer accuracy to $\sim 10^{-12}$ wavelengths. For the Hankel function form the minimum R_1 is about 10^{-5} wavelengths due to the pole at $\lambda\rho = 0$.

The numerical integration results for small R_1 were checked against results from a series approximation [Brittingham, Miller, and Okada (1977)] and were in very close agreement. For larger values of R_1 the results from different integration contours were compared as a validation test. Results for the modified Sommerfeld integrals were also checked with normal integrals used earlier [Miller et al., (1972)]. The average time required to evaluate the integrals for a given ρ and $z+z'$ on a CDC 7600 computer is about 0.06 s.

4. THE INTERPOLATION METHOD

Although the Sommerfeld integrals may be evaluated with reasonable efficiency by the methods described above, the evaluation is still much slower than for the field of a current in free space. When they must be evaluated many times, as in the numerical solution of an integral equation for an antenna over ground, the solution time can be reduced substantially by obtaining the Sommerfeld integral values through interpolation in a precomputed table.

Since the integrals depend only on ρ and $z+z'$ a two-dimensional grid of values can be generated for the field components of Eqs. (8a) through (8e) and bivariate interpolation used to obtain values for integration over a current distribution.

To facilitate interpolation in the region of the $1/R_1$ singularity, the components are divided by a function having a similar singularity and interpolation is performed on the ratio. The field components of Eqs. (8a) through (8e) are divided by $\exp(-jkR_1)/R_1$ to remove the singularity and the free-space phase factor before interpolation. The factors $\sin\phi$ or $\cos\phi$ are also omitted until after interpolation to avoid introducing the ϕ dependence. The functions to which interpolation is applied are then

$$I_\rho^V = C_1 R_1 \exp(jkR_1) \frac{\partial^2}{\partial\rho\partial z} k_1^2 V_{22}' , \tag{10a}$$

$$I_z^V = C_1 R_1 \exp(jkR_1)\left(\frac{\partial^2}{\partial z^2} + k_2^2\right) k_1^2 V_{22}' , \tag{10b}$$

$$I_\rho^H = C_1 R_1 \exp(jkR_1) \left(\frac{\partial^2}{\partial\rho^2} k_2^2 V_{22}' + k_2^2 U_{22}'\right) , \tag{10c}$$

$$I_\phi^H = - C_1 R_1 \exp(jkR_1)\left(\frac{1}{\rho}\frac{\partial}{\partial\rho} k_2^2 V_{22}' + k_2^2 U_{22}'\right) . \tag{10d}$$

After interpolation on the smoothed surfaces the results are multiplied by the omitted factors to give the correct values.

With the singularity removed, interpolation may be used for arbitrarily small values of ρ and $z+z'$. The values for $R_1 = 0$ in the interpolation grid must be found as limits for R_1 approaching zero, however, since the integrals in Eqs. 9 do not converge in this case. When ρ and $z+z'$ approach zero the dominant contributions in Eqs. (9a) through (9f) come from large λ. Hence the singular behavior can be found by setting γ_1 and γ_2 equal to λ. First, however, it is necessary to approximate D_1 and D_2 for $|\lambda| >> |k_1|$ as

$$D_1 = C_2/\lambda,\ C_2 = \frac{k_1^2 - k_2^2}{k_1^2 + k_2^2} ,$$

$$D_2 = C_3/\lambda^3,\ C_3 = \frac{k_2^2\left(k_1^2 - k_2^2\right)}{\left(k_1^2 + k_2^2\right)^2} .$$

For $|k_1|\rho << 1$ and $|k_1|(z + z') << 1$ the integrals become

$$\frac{\partial^2 V'_{22}}{\partial\rho^2} \approx C_3 \int_0^\infty \exp\left[-\lambda(z + z')\right] J_0''(\lambda\rho)\, d\lambda \tag{11a}$$

$$= C_3 \left[\frac{1 - \sin\theta}{\cos^2\theta} - 1 \right] \frac{1}{R_1} ,$$

$$\frac{\partial^2 V'_{22}}{\partial z^2} \approx C_3 \int_0^\infty \exp\left[-\lambda(z + z')\right] J_0(\lambda\rho) d\lambda = \frac{C_3}{R_1} , \tag{11b}$$

$$\frac{\partial^2 V'_{22}}{\partial \rho \partial z} \approx - C_3 \int_0^\infty \exp\left[-\lambda(z + z')\right] J'_0(\lambda\rho) d\lambda = \frac{C_3(1 - \sin\theta)}{R_1 \cos\theta} , \tag{11c}$$

$$\frac{1}{\rho} \frac{V'_{22}}{\partial \rho} \quad \frac{C_3}{\rho} \int_0^\infty \exp\left[-\lambda(z + z')\right] J'_0(\lambda\rho) \frac{1}{\lambda} d\lambda = \frac{-C_3(1 - \sin\theta)}{R_1 \cos^2\theta} , \tag{11d}$$

$$U'_{22} \approx C_2 \int_0^\infty \exp\left[-\lambda(z + z')\right] J_0(\lambda\rho) d\lambda = \frac{C_2}{R_1} , \tag{11e}$$

where

$$R_1 = \left[\rho^2 + (z + z')^2\right]^{1/2} ,$$

$$\theta = \tan^{-1}\left[(z + z')/\rho\right].$$

V'_{22} remains finite as R_1 goes to zero and hence is neglected. Equations (10a) through (10d) for R_1 equal to zero are then

$$I^V_\rho = C_1 C_3 k_1^2 \left(\frac{1 - \sin\theta}{\cos\theta} \right) , \tag{12a}$$

$$I^V_z = C_1 C_3 k_1^2 , \tag{12b}$$

$$I^H_\rho = C_1 k_2^2 \left[C_2 - C_3 + C_3 \left(\frac{1 - \sin\theta}{\cos^2\theta} \right) \right] , \tag{12c}$$

$$I^H_\phi = C_1 k_2^2 \left[C_2 - C_3 \left(\frac{1 - \sin\theta}{\cos^2\theta} \right) \right] . \tag{12d}$$

Since the limiting values as R_1 goes to zero are functions of θ it is convenient to use R_1 and θ as the interpolation variables rather than ρ and $z+z'$.

Numerical studies of the functions in Eqs. 12 for various ground parameters and frequencies have shown them to be well behaved and in general slowly varying. Typical plots are shown in Figs. 5 through 8. When the ground loss is small an evanescent wave with the lower medium wavelength is evident along the interface, as shown in Fig. 9, and may require shorter interpolation intervals in R_1, if ε_1 is large. As its wavelength becomes shorter, however, the evanescent wave is concentrated closer to the interface, reducing the region of rapid variation. When the loss tangent is on the order of 0.5 or greater the variation at the lower medium wavelength is only seen for small R_1 as in Figs. 5 through 8 where the loss tangent is 0.45.

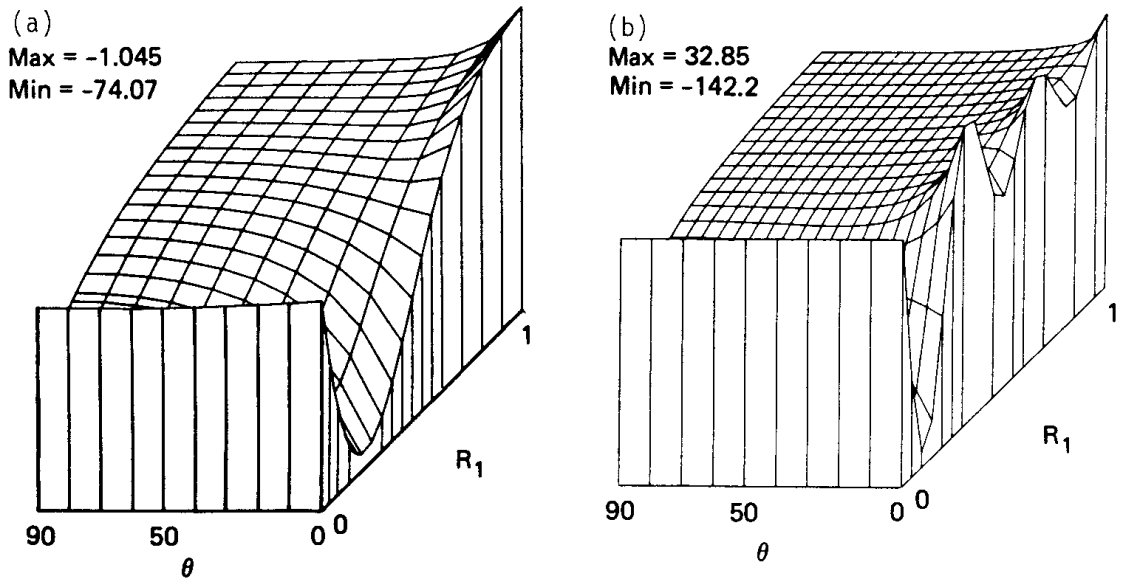

Fig. 5. Rear Part of I_ρ^H for Frequency = 10 MHz and (a) $\varepsilon_1/\varepsilon_0$ = 4 and σ_1 = 0.001 ℧/m and (b) $\varepsilon_1/\varepsilon_0$ = 16 and σ_1 = 0.

For accurate interpolation on these functions the region from 0 to 1 wavelength in R_1 was divided into three grids as shown in the following table:

Grid	Range	ΔR_1	$\Delta\theta$
1	$0 < R_1 < 0.2\lambda_0$ $0 < \theta < 90^o$	$0.02\lambda_0$	10^o
2	$0.2\lambda_0 < R_1 < 1.0\lambda_0$ $0 < \theta < 20^o$	0.05λ	5^o
3	$0.2\lambda_0 < R_1 < 1.0\lambda_0$ $20^o < \theta < 90^o$	$0.1\lambda_0$	10^o

Bivariate cubic interpolation is used on a four by four point region containing the point of interest. The grid intervals were chosen to limit the relative error to about 10^{-3} to 10^{-4} for the ground parameters of Figs. 5 through 8. The grid appears usable to at least ε_1 = 16 with low loss and ε_1 = 81 with a loss tangent of 1.

Our field evaluation uses variable-interval-width Romberg integration over the current distribution. At each integrand evaluation, the components I^V_ρ, I^V_z, I^H_ρ, and I^H_ϕ are obtained by interpolation, and the field components are combined according to the direction of the current. The numerical integral is then combined with the free-space field and with the image field multiplied by $(k_1^2 - k_2^2)/(k_1^2 + k_2^2)$ to obtain the total field over ground.

When R_1 from the observation point to the center of a wire segment is greater than one wavelength, the field is evaluated by Norton's (1937) asymptotic approximations rather than the above method. Although they are less accurate than the Sommerfeld integral forms and require longer to evaluate than the interpolation, their use permits truncating the interpolation tables. Another approximation used for R_1 greater than a wavelength is to treat the current distribution on a segment as a lumped current element with the correct moment rather than integrating over the current distribution.

5. CAPABILITIES, LIMITATIONS, AND REPRESENTATIVE RESULTS

The interpolation procedure outlined above to obtain Sommerfeld-integral values is a general one useful for various applications. When it is combined with an integral equation in particular, it provides a way to model objects near an interface such as the earth's surface. We have incorporated the interpolation procedure into a general-purpose, wire modeling program known as NEC (Numerical Electromagnetics Code) [Burke and Poggio (1977, 1980); Burke et al., (1979)]. The capabilities of this modified code and its limitations are outlined below, followed by some representative results.

5.1. Capabilities

NEC combines an electric field integral equation for wires and a magnetic field integral equation for surfaces using sine-cosine-constant basis functions respectively, for each. Delta-function weights are used for the boundary condition on both wires and surfaces. Other features include: [Burke and Poggio (1977)] 1) excitation via voltage sources on wires, an incident field with linear or elliptic polarization or the field of a Hertzian dipole in the vicinity of the antenna; 2) loads modeled by modifying the E field boundary condition; 3) structure symmetry, (either reflection or rotation) used to reduce computation time; (4) tape or disk files used for large interaction matrices; 5) partitioned-matrix method to add to a previously solved model; 6) options to use the interpolation method with Sommerfeld integrals, or the reflection coefficient approximation for lossy ground or an image for perfectly conducting ground.

For the Sommerfeld method the interpolation table is computed and stored on a file by a separate program that evaluates the Sommerfeld integrals. The table depends only on ε_1 and $1/\omega$ and may be saved for use with any antenna having the correct ground parameters. The time to compute the table is about 15 seconds on a CDC 7600 computer or about the time to model a 5 segment wire if the Sommerfeld integrals are computed directly rather than by interpolation. Using the interpolation approach, the time to compute the interaction matrix for a structure near ground is about 4 to 5 times that for a structure in free space. Solution time for the matrix equation is not changed.

The interpolation method permits accurate treatment of horizontal wires within 10^{-6} wavelengths of the interface if the radius is sufficiently small for the thin-wire approximation to be valid. If a wire end contacts the interface the current is forced to have zero derivative as a crude model for a ground stake. This condition is accurate for a perfectly conducting ground and provides accurate radiation pattern, but not impedance, for an antenna driven against a lossy ground.

NEC also includes the reflection coefficient approximation and methods for modeling ground screens via an effective surface impedance. Only the reflection coefficient method can be used for surface structures at the present time. Computation time to fill the interaction matrix by this method is two times that for free space.

5.2. Limitations

There remain several factors which limit the applicability of the present model, due either to the formulation and numerical procedures used, or to a lack of needed results. They include [Brittingham, Miller and Okada (1978)]: 1) a limit on how close to the interface an object may be modeled due to use of thin-wire approximation; 2) a requirement that the source and observation points be on the same side of the interface because a two-dimensional interpolation grid has been used; 3) uncertainty about the condition of zero current slope assumed for a wire touching the interface; 4) inability to model a wire which penetrates the interface due to lack of an appropriate charge condition there; and 5) lack of a procedure to model a wire with a dielectric sheath.

5.3. Representative Results

Some results obtained with the NEC code for antennas over ground are shown in Figs. 6 through 12, where unless otherwise indicated, the Sommerfeld/interpolation approach has been used. In Fig. 6, the input resistance of a center-fed linear antenna is shown as a function of height above ground using the Sommerfeld/interpolation method. The outcome of using the reflection coefficient approximation (RCA) for the same problem is illustrated in Fig. 7. The RCA results are reasonably accurate when the antenna is at least 0.1 to 0.2 wavelengths above the interface but are increasingly inaccurate for smaller heights, with the input resistance becoming negative for ground conductivities in the range of .01 and .04 mhos/m. The inadequacy of the RCA to treat a Beverage antenna is demonstrated in Fig. 8 where it produces a current that grows with distance from the source. By contrast, the correct Sommerfeld/interpolation results show a decaying current. Current distributions on a longer beverage antenna are shown in Fig. 9, with the resulting radiation patterns given in Figs. 10 and 11. As a last result, the attenuation of the current along an asymmetrically excited horizontal antenna over ground is compared with that for the same antenna in free-space in Fig. 12.

6. CONCLUSIONS

In this paper we have discussed the general problem of treating conducting objects near a planar interface such as the earth's surface, and have presented a specific numerical approach that permits both accurate and efficient modeling of wire antennas and scatterers in such an environment. The basis for our approach is provided by the Sommerfeld integrals in combination with a Pocklington-type, thin-wire electric-field integral equation, which is solved by the method of moments. Two additional developments have been essen-

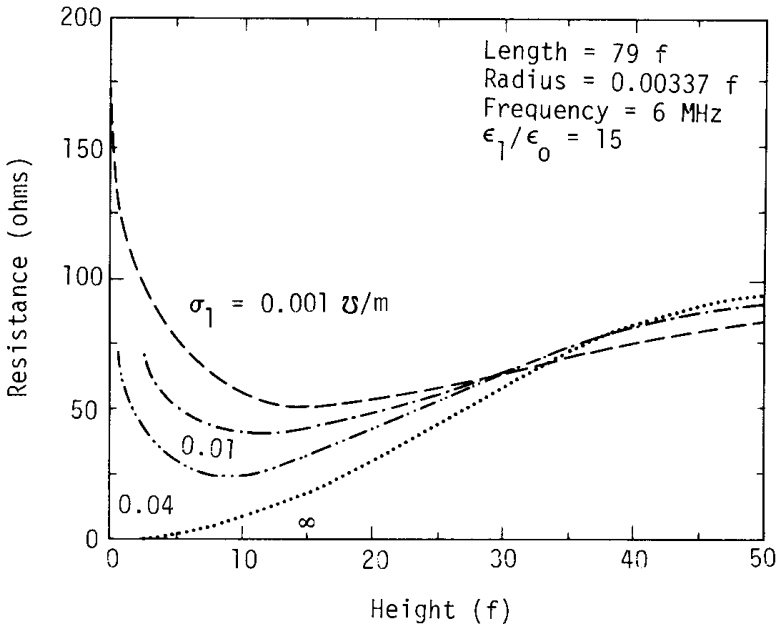

Fig. 6. Input resistance of a center-fed, horizontal dipole as a function of height above various grounds as obtained using the Sommerfeld/interpolation approach. Note the increasing resistance for all but the perfect ground as zero height is approached.

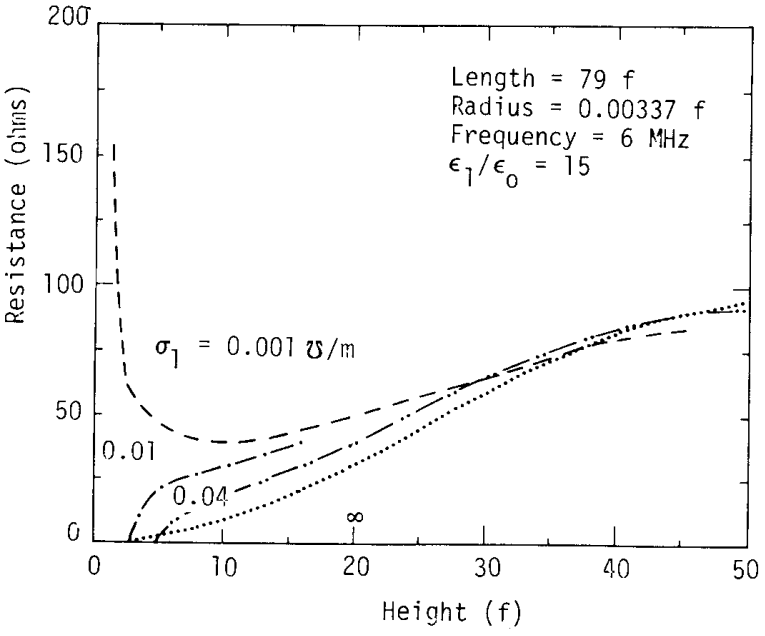

Fig. 7. Input resistance of a center-fed horizontal dipole as a function of height above various grounds as obtained using the reflection - coefficient approximation (RCA). These results are best for a low conductivity ground or perfect ground (the RCA is then exact), but lead to negative resistance for intermediate values of conductivity.

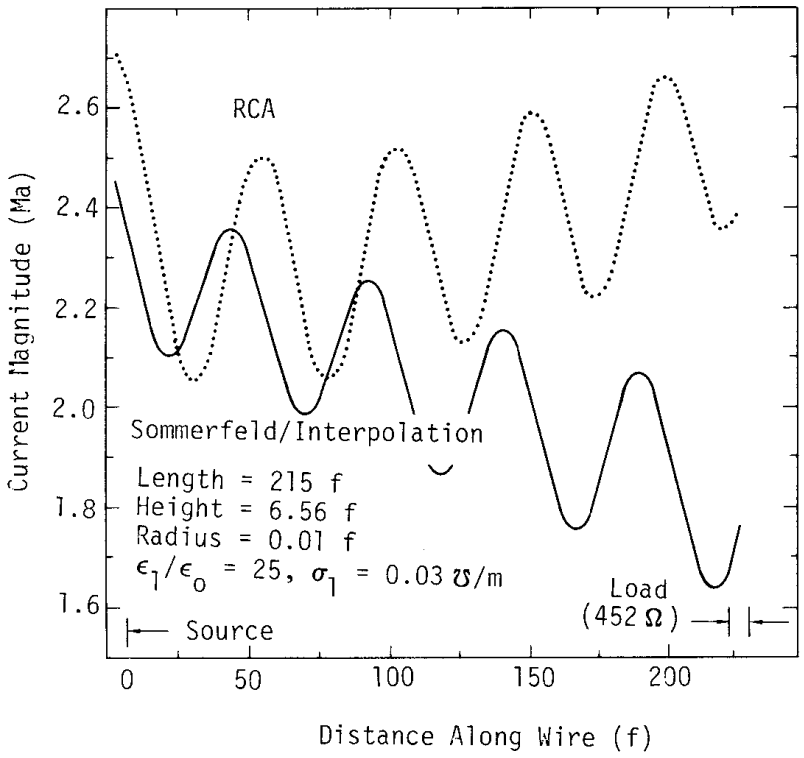

Fig. 8. Comparison of the Sommerfeld/ interpolation approach and RCA for the current distribution on a Beverage antenna. The RCA yields the non-physical result of a growing current away from the source.

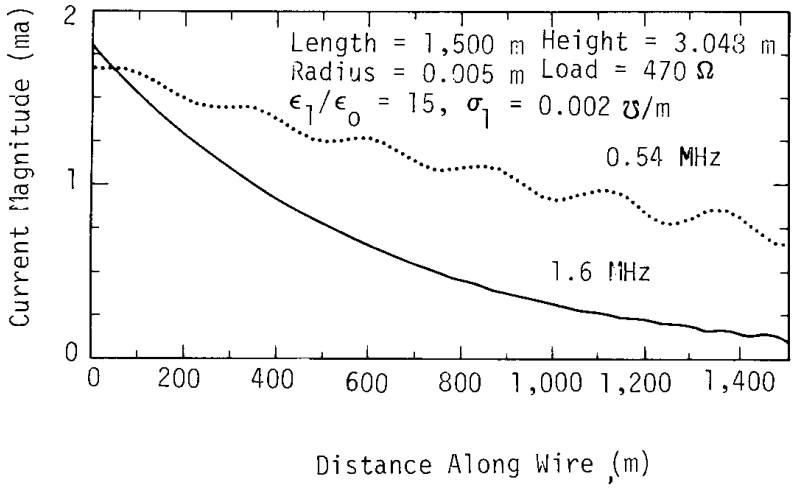

Fig. 9. Current distribution on a longer Beverage antenna at two different frequencies. As expected, increasing the frequency increases the current attenuation.

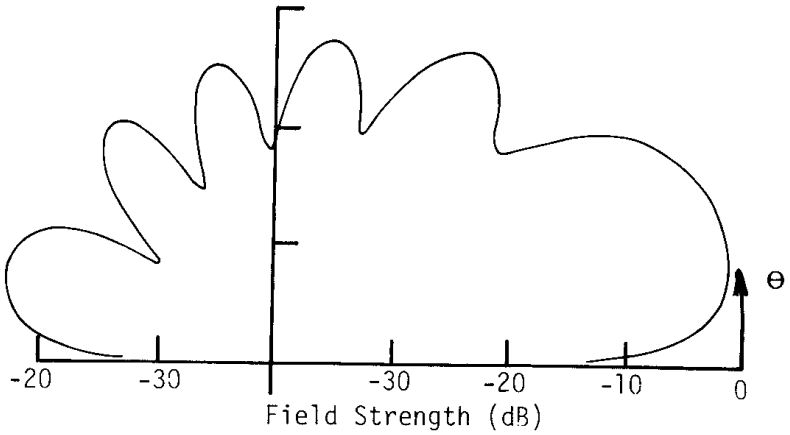

Fig. 10. Elevation plane radiation pattern of Beverage antenna of Fig. 9 for f=0.54 MHz.

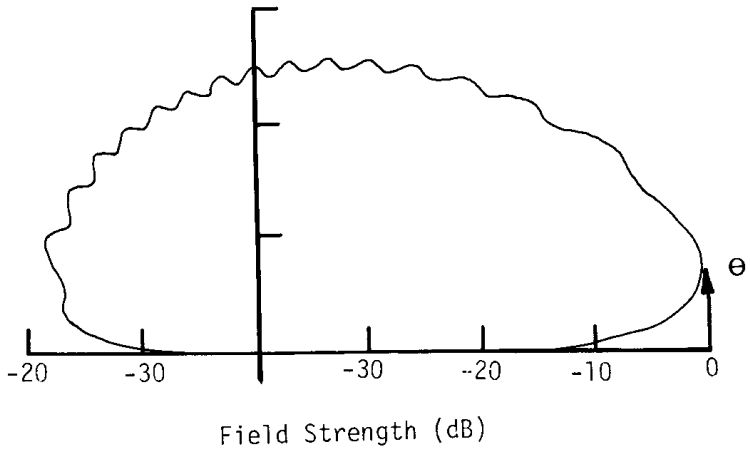

Fig. 11. Elevation plane radiation pattern of Beverage antenna of Fig. 9 for f=1.6 MHz.

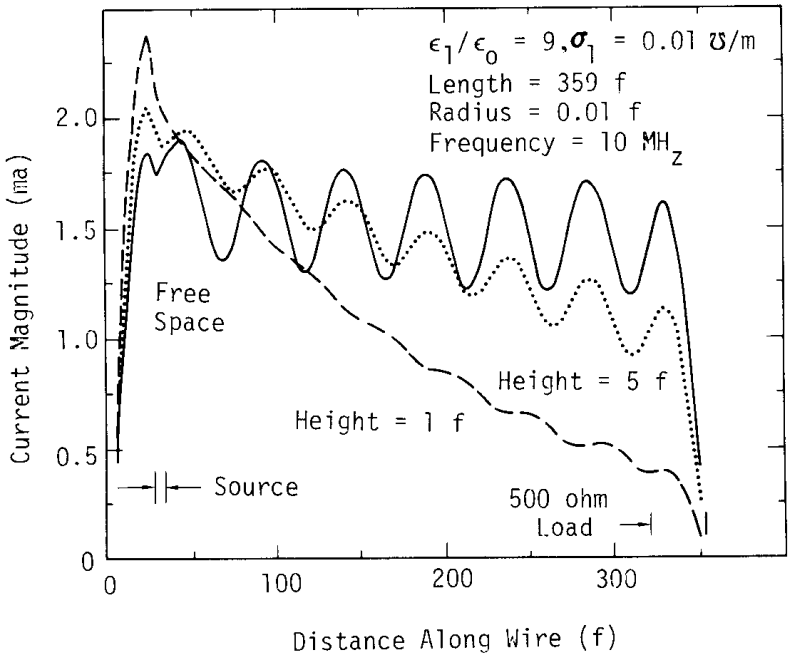

Fig. 12. Current distribution on a long asymmetrically excited antenna. Attenuation in free space is due to radiation, and increases markedly as a result of loss when the antenna is brought near the ground.

tial however, in achieving an efficient, accurate and practically useful modeling capability for objects near an interface. One is a numerical procedure for computing, reliably and accurately, Sommerfeld-integral values for arbitrarily located source-point and observation-point locations. The other is an interpolation technique which minimizes the number of such Sommerfeld integral values actually needed in modeling any object.

In general, direct computation of Sommerfeld integrals can be a time-consuming process. Furthermore, maintaining adequate accuracy over the range of the integration, can be difficult, due to the integrand varying widely as a function of both the source - observation point separation and the medium parameters. Integration contour deformation to avoid singularities and nonlinear extrapolation to speed convergence, are just two of the numerical features that have been used to develop a general-purpose computer algorithm for evaluating

Sommerfeld integrals. What results is a dependable, though relatively slow (~ 0.06 sec on a CDC 7600 computer per set of field components) procedure for obtaining the fields of elementary sources over ground.

This Sommerfeld-integral code is used to provide the field values at the intersection points of a two-dimensional grid. Values of the Sommerfeld integrals which subsequently are needed for the moment-method solution are then obtained from interpolation within this grid. This procedure provides the Sommerfeld-integral values with an accuracy comparable to, direct numerical evaluation but on the order of 1,000 times faster.

The result of these two developments is a computer model for wire antennas and scatterers located near a lossy interface that provides an accuracy comparable to that achievable for the perfect ground environment for at most a factor of two in time. This outcome is in sharp contrast to earlier models incorporating direct numerical evaluation of Sommerfeld integrals, wherein the associated computer time could be 100 or more times that for the free-space case [Miller, Poggio, Burke and Selden (1972)].

We recognize that various asymptotic expansions and other analytical techniques have been demonstrated to give accurate and efficient values for Sommerfeld integrals. But, their ranges of applicability are qenerally limited. By combining several such techniques it might be possible to develop a computational technique that would equal or exceed the capability of the interpolation approach described here, something that may well be worth doing. The specific details of the approach that is used are relatively unimportant however. What is important is that a way to handle the interface problem with acceptable accuracy and efficiency has been long needed. This need is now met, we feel, by the interpolation approach.

References

Banos, A. (1966), Dipole Radiation in the Presence of a Conducting Half Space, Pergamon Press, New York.

Brittingham, J. N., E. K. Miller and J. T. Okada (1978), "SOMINT: An Improved Model for Studying Conductivy Objects Near Conducting Half Spaces," Lawrence Livermore National Laboratory Report UCRL-52423.

Brittingham, J. N., E. K. Miller and J. T. Okada (1977), "A Bivariate Interpolation Approach for Efficiently and Accurately Modeling Antennas Near a Half Space," Electron. Lett., 13, pp. 690-691.

Burke, G. J., and A. J. Poggio (1977, revised 1980), "Numerical Electromagnetics Code (NEC) - Method of Moments," NOSC TD116.

Lytle, R. J. and D. L. Lager (1974), "Numerical Evaluation of Sommerfeld Integrals," Lawrence Livermore National Laboratory Report UCRL-51688.

Miller, E. K. (1970), "A Variable Interval Width Quadrature Technique Based on Romberg's Method," Journal of Computational Physic 5, No. 2,.

Miller, E. K., J. N. Brittingham and J. T. Okada (1978), Explicit Modeling of Antennas With Sparse Ground Screens," Electron Lett. 14, pp. 627-629.

Miller, E. K. and F. J. Deadrick (1975), "Some Computational Aspects of Thin-Wire Modeling," Chapter 4 in Numerical and Asymptotic Techniques in Electromagnetics, edited by R. Mittra, Springer-Verlag, New York.

Miller, E. K., A. J. Poggio, G. J. Burke and E. S. Selden, (1971), "Analysis of Wire Antennas in the Presence of a Conducting Half-Space: Part I. The Vertical Antenna in Free-Space," Canadian Journal of Physics, 50, pp. 879-888.

Miller, E. K., A. J. Poggio, G. J. Burke and E. S. Selden, (1972), "Analysis of Wire Antennas in the Presence of a Conducting Half Space: Part II. The Horizontal Antenna in Free Space," Canadian Journal of Physics, 50, pp. 2614-2627.

Norton, K. A., Sommerfeld (1973), "The Propagation of Radio Waves Over the Surface of the Earth and in the Upper Atmosphere," Proc. IRE, 25, No. 9, p. 1205.

Rahmat-Samii, Y., R. Mittra and P. Parhami, "Integrals for the Lossy Half-Space Problem," Electromagnetics Society Journal, 1, No. 1 (this issue).

Shanks, Daniel (1955), "Nonlinear Transformations of Divergent and Slowly Convergent Sequences," J. of Math. & Phy., pp. 1-43.